Eur. Phys. J. D **13**, 385–391 (2001)

THE EUROPEAN PHYSICAL JOURNAL D

EDP Sciences

Theoretical and experimental study of discrete behavior of Shilnikov chaos in a CO_2 laser

A.N. Pisarchik[1,a], R. Meucci[2,b], and F.T. Arecchi[2,3,c]

[1] Centro de Investigaciones en Optica, Loma del Bosque 115, Col. Lomas del Campestre, 37150 Leon, Gto., Mexico
[2] Istituto Nazionale di Ottica Applicata, L.E. Fermi 6, 50125 Firenze, Italy
[3] Department of Physics, University of Firenze, 50125 Firenze, Italy

Received 28 September 2000 and 27 October 2000

Abstract. The discrete distribution of homoclinic orbits has been investigated numerically and experimentally in a CO_2 laser with feedback. The narrow chaotic ranges appear consequently when a laser parameter (bias voltage or feedback gain) changes exponentially. Up to six consecutive chaotic windows have been observed in the numerical simulation as well as in the experiments. Every subsequent increase in the number of loops in the upward spiral around the saddle focus is accompanied by the appearance of the corresponding chaotic window. The discrete character of homoclinic chaos is also demonstrated through bifurcation diagrams, eigenvalues of the fixed point, return maps, and return times of the return maps.

PACS. 05.45.Ac Low-dimensional chaos – 05.45.Pq Numerical simulations of chaotic models – 42.55.Lt Gas lasers including excimer and metal-vapor lasers

1 Introduction

Shilnikov chaos normally appears when a parameter is varied towards the homoclinic condition associated with a saddle focus [1–3]. Its peculiarity consists in an astonishing regularity of the geometric trajectory in phase space. The chaotic motion is characterized by homoclinic orbits in the phase space with large fluctuations in the return time associated with the sensitivity of the trajectory on the initial approach to the unstable point. The return times are erratic and only an average return period can be defined. This suggests that an appropriate indicator of chaos may be the distribution of the return times to a given threshold, and the strength of chaos is associated with the amount of decorrelation between successive returns [4]. If the map of the return times is sufficient to characterize the dynamics, then such a one-dimensional (1D) dissipative map corresponds to a 3D continuous dynamics. Thus, the minimal model interpreting the homoclinic behavior is a set of three coupled variables [3] with an unstable fixed point having a pair of complex conjugate eigenvalues and a real one, with the condition that the saddle quantity be positive [2]. The appealing feature of such a model is that a local linear stability analysis around the unstable point provides a global description of the motion [5].

Shilnikov chaos [3] was previously observed in many systems, including a single mode lasers with feedback [6] and with a saturable absorber [7], the Belousov-Zhabotinskii reaction [8], a glow discharge plasma [9], an optically bistable device [10], a multimode laser [11], and some other systems. The phase diagram of a single mode CO_2 laser with feedback observed by us over many years [6] represents orbits characterized by a large damped oscillation followed by a smaller growing oscillation. This behavior seems to imply the coexistence of the two saddle foci, one corresponding to an inward spiral, followed by one corresponding to an outward spiral. We will see that this conjecture is wrong and there is only one saddle focus. In order to explore this question, we must make reference to a sound model. Referring to our experiment, a CO_2 laser with feedback belonging to class-B lasers, is described by two dynamical variables [12] (resonant population difference and light intensity) plus a third variable corresponding to a voltage signal which provides a feedback from the detector to the cavity loss modulator. This 3D model was compatible with the observations of giant spikes and the prediction of their return in terms of a return time statistics with an associated 1D dissipative map [4]. However, the 3D model is unable to account for all the features observed in the laser with feedback, therefore a more detailed description is necessary. In fact, the CO_2 resonant transition is coupled to other rotational levels, so that the complete model is 6D [13].

In this paper we study numerically and experimentally the discrete behavior of Shilnikov chaos. We reveal how changing a control parameter one can change the

[a] *On leave from* Stepanov Institute of Physics of National Academy of Sciences of Belarus.
e-mail: apisarch@foton.cio.mx
[b] e-mail: ric@ino.it
[c] e-mail: arecchi@ino.it

number of loops around the saddle focus. To our knowledge, no accurate characterization of the discrete behavior of Shilnikov chaos has been previously reported in physical systems, although the effect of discretization has been described in the mathematical literature [14]. Recently, we have reported on the first experimental observation of the discrete character of Shilnikov chaos [15]. The present work is primarily concerned with identifying regions of operation in which homoclinic chaos can be observed, even though such regions can be quite narrow. We show how these regions depend on the control parameters. We also characterize homoclinic chaos by the return map of the return times, as introduced in [4] and later applied in [16].

The paper is organized as follows. In Section 2 we describe the model equations and the results of numerical simulations to characterize the discrete behavior of Shilnikov chaos. In Section 3 we briefly comment on the experimental setup of CO_2 laser with feedback and describe the experimental results. Finally, the conclusions are presented in Section 4.

2 Numerical simulations

2.1 Model equations

Standard laser theoretical models are based on the interaction of a single mode field with a resonant molecular transition, thus requiring consideration of two molecular levels. Applying an extra degree of freedom to account for feedback, this will amount to a three-equation model [17]. However, homoclinic trajectory occurs over long times, and during these times there is a consistent population transfer from the rotational manifold of all other molecular levels, not directly coupled to the field, towards the resonant levels. This population transfer is accounted for by a four-level system [13,18], leading to a six-equation dynamical model as follows

$$\dot{x_1} = k_0 x_1 (x_2 - 1 - k_1 \sin^2 x_6), \quad (1)$$

$$\dot{x_2} = -\Gamma_1 x_2 - 2k_0 x_1 x_2 + \gamma x_3 + x_4 + P_0, \quad (2)$$

$$\dot{x_3} = -\Gamma_1 x_3 + x_5 + \gamma x_2 + P_0, \quad (3)$$

$$\dot{x_4} = -\Gamma_2 x_4 + \gamma x_5 + z x_2 + z P_0, \quad (4)$$

$$\dot{x_5} = -\Gamma_2 x_5 + z x_3 + \gamma x_4 + z P_0, \quad (5)$$

$$\dot{x_6} = -\beta x_6 + \beta B_0 - \beta f(x_1), \quad (6)$$

where $f(x_1) = Rx_1/(1 + \alpha x_1)$ is the feedback function. In these equations, x_1 is the normalized photon number proportional to the laser intensity, x_2 is proportional to the population inversion, x_3 is proportional to the sum of the populations on the two resonant levels, x_4 and x_5 are proportional, respectively, to difference and sum of the populations of the rotational manifolds coupled to the lasing levels. We assume that each manifold contains $z = 10$ sublevels. The variable x_6 is proportional to the feedback voltage that affects the cavity loss parameter through the relation $k_0(1 + k_1 \sin^2 x_6)$. The time t is rescaled to $\tau = t\gamma_R$, where γ_R is a suitable collision relaxation rate ($\gamma_R = 7 \times 10^5$ s^{-1}). The control parameters B_0 and R are proportional to the bias voltage and the gain of the feedback, respectively. The parameters Γ_1, Γ_2, γ, and β represent decay rates, α is a saturation factor of the feedback loop, and P_0 is the pump parameter. The fixed parameter values are collected in Table 1. They correspond to accurate measurements performed on the used experimental system [13].

Table 1. Parameter values used in simulations.

Γ_1	10.0643	α	32.8767	k_0	28.5714	γ	0.05
Γ_2	1.0643	β	0.4286	k_1	4.5556	P_0	0.016

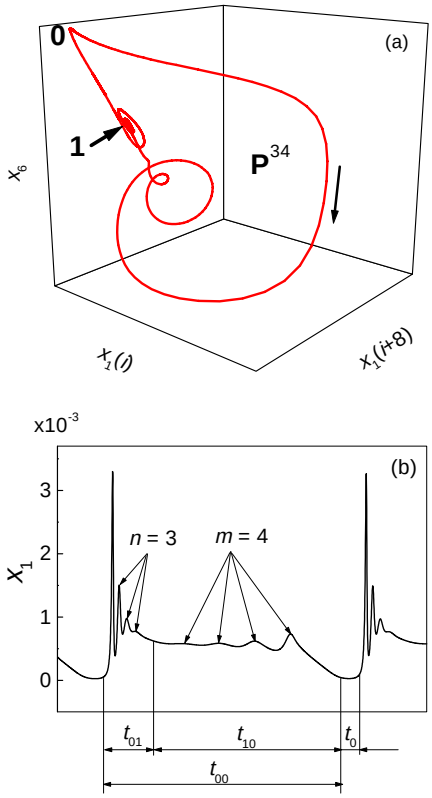

Fig. 1. (a) Numerical phase space trajectory on the 3D projection of the 6D space. $B_0 = 0.1026$. $R = 160$. It results partly from embedding and partly from the plot of two different degrees of freedom. (b) Corresponding time series of the laser intensity and definitions of the characteristic times t_{01}, t_{10}, t_{00}, and t_0. The large and small oscillations corresponding to the inward and outward spiral loops are indicated by the arrows.

2.2 Phase space geometry

The dynamical behavior of the CO_2 laser with feedback is strongly determined by the presence of two fixed points in the phase space shown in Figure 1a. For the laser intensity which is the variable usually observed in the experiment [4,6,12,15], these fixed points, defined as 0 and 1,

are characterized, respectively, by a zero and non zero intensities. The time evolution of the laser intensity is represented by an orbit in the phase space of the laser variables winding around these two fixed points with the particular feature of an inward spiral motion approaching point 1 and an outward spiral motion leaving the same point.

The trajectory shown in Figure 1a is the 3D projection of a bi-periodic P^{nm} oscillations evaluated by the 6D model. The index n denotes the number of the loops in the inward spiral while the index m is the number of the outward spiral loops. The system of equations (1–6) possesses a homoclinic orbit Γ_0 connecting fixed point 0 to itself.

The most common time-dependent regime for the output power of the laser with feedback is composed of coexisting narrow large and small spikes repeating regularly at a period $T = t_{00} + t_0$ as shown in Figure 1b. The duration times associated with the inward and outward spirals are called respectively t_{01} and t_{10} and the overall (return) time of the homoclinic cycle is denoted as t_{00}. After a time interval t_0 spent near point 0, the next homoclinic cycle starts. By varying the control parameters one can change the number of the loops n and m, or, in other words, the type of periodicity. Each change in the number of the outward spiral loops m is accompanied by a chaotic motion C^j $(j = 1, 2, 3, ...)$ [15]. The regime of Shilnikov chaos may be described in the phase space through a quasi-homoclinic orbit Γ_1, leaving fixed point 1 and reinjected into that point. This connection occurs within very narrow parameter range. In this regime the number of the outward spiral loops depends on how close the trajectory approaches fixed point 1 after the reinjection. Therefore, at the chaotic regime the time t_{10} varies from one period T of the homoclinic cycle Γ_0 to the another. Theoretically, the number of quasi-homoclinic cycles Γ_1 increases without a limit as the system approaches the homoclinic bifurcation. Thus, the fixed point 1 is responsible for homoclinic chaos.

2.3 Eigenvalues

The dynamics of the system depends sensitively on the relative values of the eigenvalues of the saddle focus located in the origin 1. The inward spiral motion towards the unstable saddle focus 1 is related to a non stationary solution of the equation model characterized by a stable manifold with complex eigenvalues $(-\rho_1 \pm i\omega_1)$. The fixed point 1 has four real and two complex conjugates eigenvalues. These last two $(\rho_2 \pm i\omega_2)$ account for the unstable manifold of this point. For a homoclinic orbit such as Γ_1 associated with a saddle focus such as point 1, Shilnikov showed that, if in the neighborhood of this point the characteristic time of the flow following the focus directions is the largest one ($\rho_2/\lambda_2 > 1$, where λ_2 is the smallest real eigenvalue), the system represents a chaotic behavior [3]. However, as was shown by Tresser [19], chaos may appear even if this condition is not fulfilled. This happens if the unstable and the stable manifolds are not perfectly connected but close to form a homoclinic orbit.

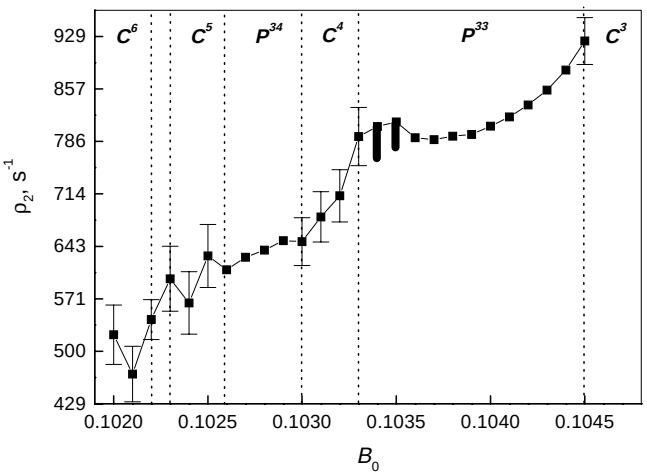

Fig. 2. Real part of the eigenvalue ρ_2 of fixed point 1 *versus* bias voltage B_0 at $R = 160$.

In Figure 2 we show that the real part of the eigenvalue ρ_2 increases monotonically with bias voltage B_0, while ρ_1 remains constant, $\rho_1 = 3.27 \times 10^3$ s^{-1}. One can observe the succession of periodic P^{nm} and chaotic windows C^j as B_0 is changed. The number j of a successive chaotic regime is defined to be equal to the number of the outward spiral loops m in a bi-periodic regime preceding this chaotic window. The boundaries between periodic and chaotic regimes are indicated in the figure by the vertical dashed lines. We have added error bars within C^j ranges, since the reported values are an average over several occurrences, *i.e.* over several homoclinic cycles Γ_0. In the periodic window between C^3 and C^4, the simultaneous presence of different periods is represented by the broader marks.

2.4 Bifurcation diagrams

Numerical bifurcation diagrams of the laser intensity with respect to the control parameters R and B_0 are shown in Figures 3 and 4. For each parameter value successive maxima of the x_1 variable are plotted. This allows us to characterize the discrete behavior of periodic and chaotic orbits. The calculated diagrams are close to the experimentally observed behavior.

As seen from the diagrams, the laser dynamics develops with a change in the parameter values in the following way. At large R (Fig. 3) and small B_0 (Fig. 4) the laser operates in a cw (steady-state) regime. This behavior is connected to the chaotic regime by a subharmonic cascade, terminated by chaos around fixed point 1. At low R (Fig. 3, regimes $n = 1 \dashrightarrow 5$) and high B_0 (Fig. 4, $B_0 > 0.12$) only the inward spiral exists. This means that, for these values of the parameters, fixed point 1 has no effect on the laser dynamics, and hence chaos does not appear. As seen from the figures, the increase in the gain R leads to discrete increments of the number of the loops n of fixed point 1, while the change in B_0 does not result in a change in n (see Fig. 4).

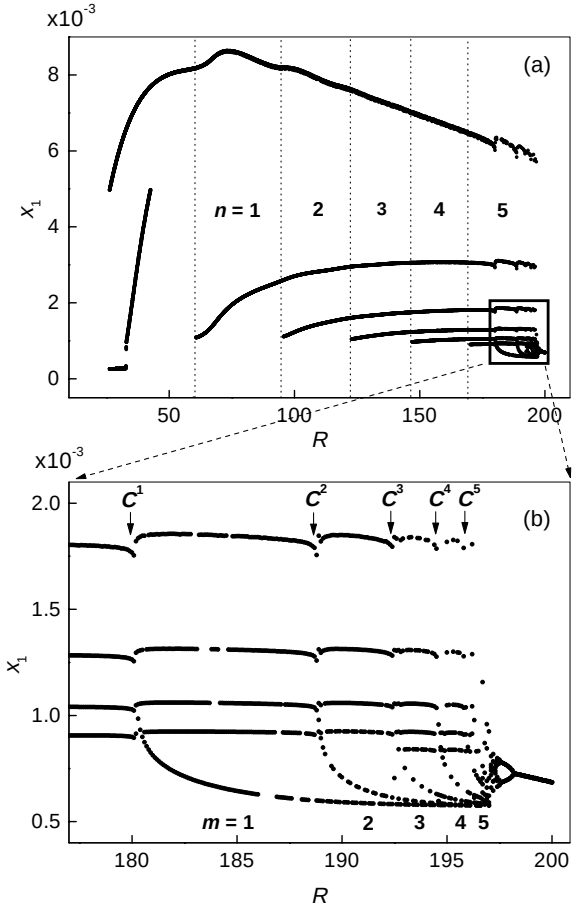

Fig. 3. (a) Numerical bifurcation diagram of the laser intensity with feedback gain R as a control parameter at $B_0 = 0.12$. (b) Enlarged part of the diagram.

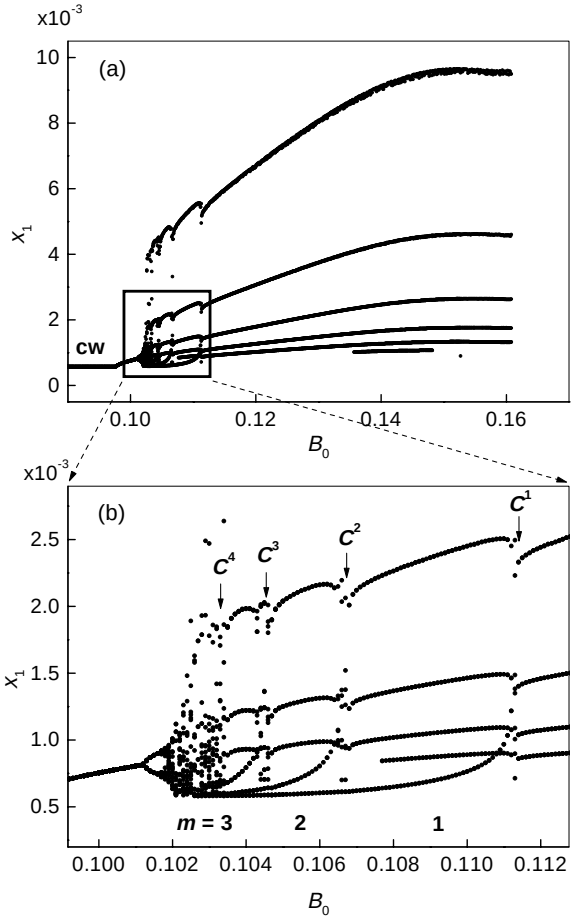

Fig. 4. (a) Numerical bifurcation diagram of the laser intensity with bias voltage B_0 as a control parameter at $R = 160$. (b) Enlarged part of the diagram.

At high R and low B_0 a new outward spiral arises around point 1. That is, at $R > 180$ (Fig. 3b) besides the inward spiral around point 1, which by now has reached the value $n = 5$, spirals around point 1 also appear. They give rise to homoclinic chaos C^j located within some narrow parameter ranges. Away from these chaotic windows, bi-periodic regimes P^{nm} take place. Between P^{nm} and $P^{n(m+1)}$ periodic states there always exists a chaotic state C^j. The widths of periodic P^{nm} windows get smaller as m increases. This explains why in experiments it is difficult to observe large m numbers: the width of the periodic window becomes of the same order of magnitude as experimental noise.

2.5 Periodicity

In Figure 5 we show how the number of loops depends on the control parameters. We have found that the n-periodic regions are distributed approximately equidistantly with the feedback gain R (Fig. 5a), while m-periodic regions and chaotic regions are separated exponentially with the bias voltage B_0 (Fig. 5b). Each steep change of m is accompanied by the very narrow chaotic regions C^j indicated by the arrows, where j is the number of a chaotic

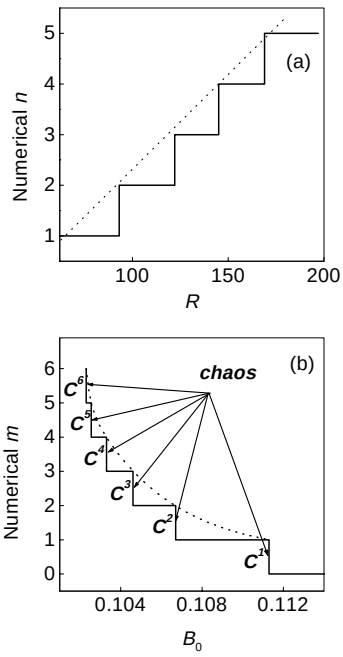

Fig. 5. (a) Calculated number of loops n *versus* feedback gain R at $B_0 = 0.12$ and (b) m *versus* bias voltage B_0 at $R = 160$.

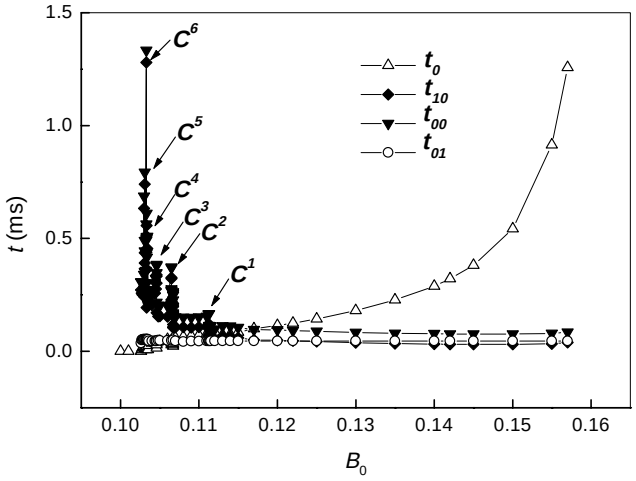

Fig. 6. Numerical return times for fixed points 0 and 1 *versus* bias voltage B_0 at $R = 160$.

state that corresponds to the number of the loops m around fixed point 1. We have found up to 6 homoclinic chaotic states, since the maximum observed loops m was 6.

2.6 Return times

The return time maps are an extremely convenient tool for analyzing homoclinic chaos [4,16]. Rather than looking at the reconstructed phase space trajectory, the information is derived directly from the time evolution of the signal. In Figure 6 we show the dependence of the return times on B_0. One can see that t_{01} and t_0 change monotonically with B_0 and hence they are not related to chaos. On the contrary t_{10} and as a consequence t_{00}, shows strong oscillations as B_0 changes and the chaotic regimes are characterized by the coexistence of many t_{00} and t_{10} values for the same B_0. The deviation of these times increases with j.

We recall (see [4,17]) that a map of the global return times can be built by the local analysis around the saddle focus. A map of the global return time in the chaotic regime is made of many oscillations crossing the diagonal straight line of the plane (t_{n+1}, t_n) (locus of fixed points) at angles much larger than 45°, thus showing very high local expansion rates. As a result, tiny changes in a control parameter may induce dramatic changes in the range of return times.

The numerical return map of return times (RMRT) corresponding to chaos C^5 is shown in Figure 7a. This map is derived from the temporal evolution of the laser intensity shown in Figure 7b. We consider the intersections with the surface of constant intensity ($x_1 = 5.8 \times 10^{-4}$) that cuts all oscillations whenever $\mathrm{d}x_1/\mathrm{d}t < 0$ [16]. Then we determine the times t_i between successive intersections. All the RMRT, *i.e.*, the plot t_i *vs.* $i + 1$, present a multivalued structure.

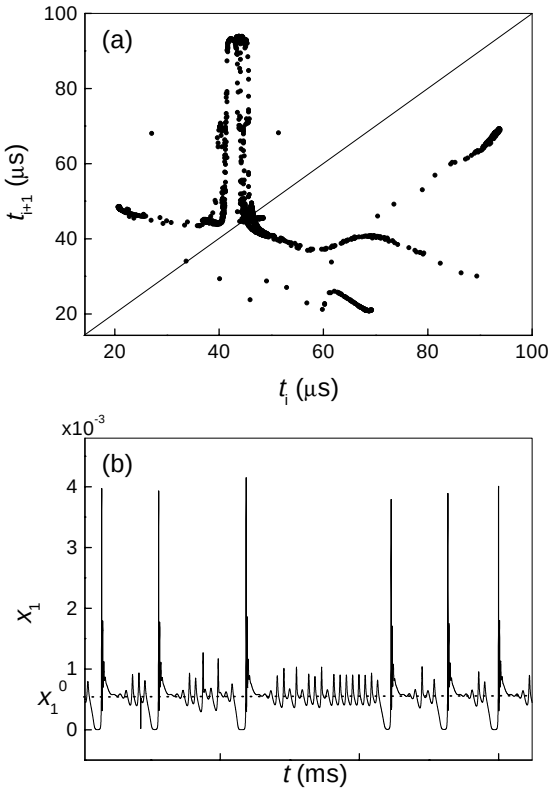

Fig. 7. (a) RMRT (return map of return times) for C^5 for model equations (1–6). $5{\times}10^5$ points have been analyzed during 70 ms. (b) Portion of the time series including $x_1^0 = 5.8 \times 10^{-4}$ at which the signal was sampled.

3 Experiment

3.1 Setup

The experiments reported on this paper have been carried on a single mode CO_2 laser with feedback. The experimental setup was already described elsewhere [17]. An intracavity loss modulator is driven by a bias voltage B, which acts as a control parameter, plus a signal feedback from a detector inspecting the amount of output intensity, and amplified by a factor A. A is the second control parameter. Thus, the laser with feedback represents an autonomous system, where the feedback provides an additional degree of freedom, which is necessary to observe chaos.

The relationship between the parameter B_0 in equation (6) and the experimental bias voltage B is $B_0 = \pi(B - V_0)/V_\lambda$, where $V_0 = 100$ V and $V_\lambda = 4240$ V.

3.2 Phase space diagram

The experimental phase diagram is shown in Figure 8. One can see the very close similarity with the numerical trajectory shown in Figure 1a. So far the previous experiments and their interpretation have covered separately either the occurrence of the giant spikes [6,17] or the small oscillations around the saddle focus 1, as well as ways of stabilizing them [18].

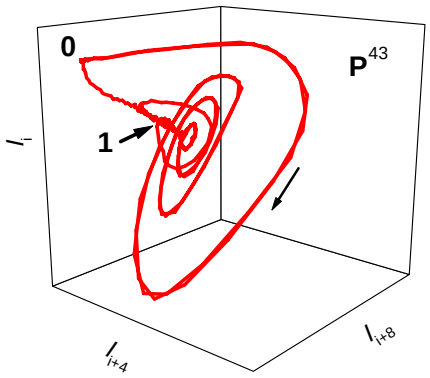

Fig. 8. Experimental phase space trajectory in CO_2 laser with feedback. Bias voltage $B = 210$ V. Feedback gain $A = 2055$. The phase space is built by an embedding technique with appropriate delays.

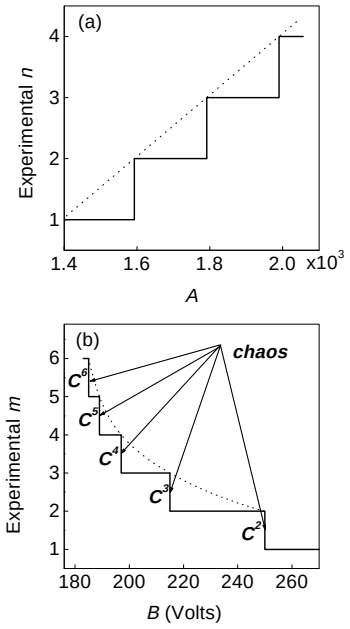

Fig. 9. Experimental number of (a) inward spiral loops n *versus* feedback gain A at bias voltage $B = 210$ V and (b) outward spiral loops m *versus* bias voltage B at feedback gain $A = 1730$.

3.3 Discretization of chaos

In Figure 9 we show how the number of loops, observed experimentally, depends on the control parameters. One can see that these experimental results qualitatively agree with the numerical results shown in Figure 5. As in the calculations we have found up to 6 homoclinic chaotic states which are separated exponentially with the bias voltage (see Fig. 9b).

The experimental RMRT corresponding to chaos C^5 is shown in Figure 10. As in the numerical simulations this map is derived from the temporal evolution of the laser intensity and represents a multi-valued structure. These maps are quite different from those reported in [4], which were taken setting a high threshold value, and thus reporting the occurrence of the highest spikes. In [4] no detail

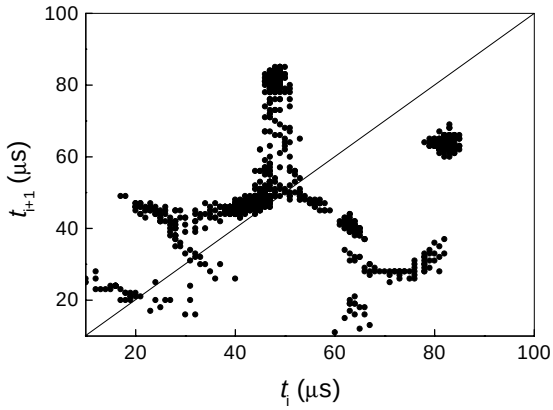

Fig. 10. Experimental RMRT for C^5.

on the number of loops around saddle focus 1 could be obtained.

4 Conclusions

The discrete behavior of homoclinic chaos has been studied numerically and experimentally in a CO_2 laser with feedback. We have shown that chaotic regions are separated exponentially as a control parameter is varied. The occurrence of a homoclinic window is accompanied by a change in the number of loops m in the outward spiral around the saddle focus 1 responsible for Shilnikov chaos. Instead, the number of loops n in the inward spiral is not associated with chaos and changes equidistantly with a control parameter.

Furthermore, the performed return time analysis confirms the discrete character of homoclinic chaos, with a satisfactory agreement between numerical and experimental results. This discrete character had already been observed in Belousov-Zhabotinskii reaction [8], however the exponential dependence of periodic and chaotic windows is here demonstrated numerically and experimentally for the first time. In conclusion, while previous works monitored the overall return time [4] or stabilized fixed point 1 [13] or just the first limit cycle around it [18], here for the first time we provide the parameter value for the onset of different number of loops around the saddle focus.

This work has been supported in part by Consejo Nacional de Ciencia y Tecnología de México (CONACYT) (project No. 33769-E) and through a grant from the Institute Mexico-USA of the University of California (UC MEXUS) and CONACYT. A.N.P. acknowledges support from CONACYT through Cátedra Patrimonial (Ref. 990457) and thanks R. Herrero and G. Orriols for useful discussions. We also thank L. Calero and E. Allaria for their assistance in the experimental data collection and A. DiGarbo for helpful discussions.

References

1. S. Wiggins, *Global Bifurcations and Chaos – Analytical Methods* (Springer-Verlag, New York, 1984).
2. Y.A. Kuznetsov, *Elements of Applied Bifurcation Theory* (Springer-Verlag, New York, 1995).

3. L.P. Shil'nikov, Sov. Math. Dokl. **6**, 163 (1965); Math. USSR Sbornik **10**, 91 (1970).
4. F.T. Arecchi, A. Lapucci, R. Meucci, J.A. Roversi, P.H. Coullet, Europhys. Lett. **6**, 677 (1988).
5. A. Arneodo, P.H. Coullet, E.A. Spiegel, C. Tresser, Physica D **14**, 327 (1985).
6. F.T. Arecchi, R. Meucci, W. Gadomski, Phys. Rev. Lett. **58**, 2205 (1987).
7. D. Hennequin, F. de Tomasi, B. Zambon, E. Arimondo, Phys. Rev. A **37**, 2243 (1988); D. Dangoisse, A. Bekkali, F. Papoff, P. Glorieux, Europhys. Lett. **6**, 335 (1988).
8. F. Argoul, A. Arnéodo, P. Richetti, J. Chem. Phys. **84**, 1367 (1987).
9. T. Braun, J.A. Lisboa, J.A.C. Gallas, Phys. Rev. Lett. **68**, 2770 (1992).
10. R. Herrero, F. Boixader, G. Orriols, J.I. Rosell, F. Pi, Opt. Commun. **112**, 324 (1994).
11. E.A. Viktorov, D.R. Klimer, M.A. Karim, Opt. Commun. **113**, 441 (1995).
12. F.T. Arecchi, in *Instabilities and Chaos in Quantum Optics*, edited by F.T. Arecchi, R.G. Harrison (Springer-Verlag, Berlin, 1987).
13. M. Ciofini, A. Labate, R. Meucci, M. Galanti, Phys. Rev. E **60**, 398 (1999).
14. P. Gaspard, G. Nicolis, J. Stat. Phys. **31**, 499 (1983); P.P. Glendinning, C.S. Sparrow, *ibid.* **35**, 545 (1984); J.W.-J. Beyn, in International. Series of Numerical Mathematics **79** (Birkhäuser Verlag, Basel, 1987), p. 1.
15. A.N. Pisarchik, R. Meucci, F.T. Arecchi, Phys. Rev. E **62**, 8823 (2000)
16. A.R. Zeni, T. Braun, R.R.B. Correia, P. Alcantara Jr, L. Guidoni, E. Arimondo, Phys. Rev. E **57**, 288 (1998).
17. F.T. Arecchi, W. Gadomski, A. Lapucci, H. Mancini, R. Meucci, J.A. Roversi, J. Opt. Soc. Am. B **5**, 1153 (1988).
18. R. Meucci, A. Labate, M. Ciofini, Phys. Rev. E **56**, 2829 (1997).
19. C. Tresser, Ann. Inst. Henry Poincaré **40**, 441 (1964).